Phenomenological Description of a Three-Center Insertion Reaction: An Information-Theoretic Study

Rodolfo O. Esquivel,*[,†,‡,||] Nelson Flores-Gallegos,[†] Jesús S. Dehesa,[‡,||] Juan Carlos Angulo,[‡,||] Juan Antolín,[§,||] Sheila López-Rosa,[‡,||] and K. D. Sen[⊥]

Departamento de Química, Universidad Autónoma Metropolitana-Iztapalapa, 09340, México D.F., Departamento de Física Atómica, Molecular y Nuclear, Universidad de Granada, 18071-Granada, Spain, Departamento de Física Aplicada, EUITIZ, Universidad de Zaragoza, 50018-Zaragoza, Spain, Instituto Carlos I de Física Teórica y Computacional, Universidad de Granada, 18071-Granada, Spain, and School of Chemistry, University of Hyderabad, Hyderabad 500046, India

Received: September 14, 2009; Revised Manuscript Received: November 25, 2009

Information-theoretic measures are employed to describe the course of a three-center chemical reaction in terms of detecting the transition state and the stationary points unfolding the bond-forming and bond-breaking regions which are not revealed in the energy profile. The information entropy profiles for the selected reactions are generated by following the intrinsic-reaction-coordinate (IRC) path calculated at the MP2 level of theory from which Shannon entropies in position and momentum spaces at the QCISD(T)/6-311++G(3df,2p) level are determined. Several complementary reactivity descriptors are also determined, such as the dipole moment, the molecular electrostatic potential (MEP) obtained through a multipole expansion (DMA), the atomic charges and electric potentials fitted to the MEP, the hardness and softness DFT descriptors, and several geometrical parameters which support the information-theoretic analysis. New density-based structures related to the bond-forming and bond-breaking regions are proposed. Our results support the concept of a continuum of transient of Zewail and Polanyi for the transition state rather than a single state, which is also in agreement with reaction-force analyses.

Introduction

Theoretical studies of potential-energy surfaces, a subject of increasing interest, have been performed at various levels of sophistication in an attempt to understand the stereochemical course of chemical reactions.[1] Particular interest has been focused on extracting information about the stationary points of the energy surface. In the Born–Oppenheimer framework, (i) minima on the *N*-dimensional potential-energy surface for the nuclei can be identified with the classical picture of equilibrium structures of molecules, and (ii) saddle points can be related to transition states (TSs) and reaction rates. Since the formulation of TS theory,[2,3] a great effort has been devoted to developing models to characterize TSs. This theory is assumed to govern the height of a chemical reaction barrier, so that any insight into the nature of the TS are likely to provide deeper understanding of the chemical reactivity. Computational quantum chemistry has sidestepped the inherent problems by managing rigorous mathematical definitions of critical points on a potential-energy hypersurface and hence assigned them to equilibrium complexes or TSs. Within this approach, minima and saddle points have been fully characterized through the first and second derivatives of the energy (gradient and Hessian) over the nuclei positions.[4]

Although critical points of the energy surface are useful mathematical features for analyzing the reaction path, their chemical or physical meaning remains uncertain.[5] In the search for providing with a more intuitive quantum chemical basis of the mathematical saddle point, Shaik[6] developed a general model for the TS of a chemical reaction based on the valence-bond theory (VB) through the avoided crossing state (ACS) or the perfectly resonating state (PRS) of the VB configurations that describe a chemical transformation.[7] Considering that the TS is a species which varies, geometrically and electronically, in a continuous manner among the well-defined structures of reactants, products, and potential intermediates, it would then be important to obtain more chemically meaningful information about the process in the vicinity of the TS, where the ion-complex species involved in the chemical reaction exert physically important phenomena such as bond breaking or bond forming and charge depletion or charge accumulation. This information would be of great value too in assessing whether the ACS/PRS is located on the reaction profile which descends from the saddle point along the reaction vector and in assisting in the locating/designing of PRSs which may enable to trace on the pathways of the chemically meaningful potential hypersurface. With the advent of femtosecond time-resolved methods, the aforementioned theories have turned out to be more relevant at the present time.[8] Femtochemistry techniques have been applied to chemical reactions ranging in complexity from bond breaking in diatomic molecules to dynamics in larger organic and biological molecules, providing new insight into the understanding of fundamental chemical processes. Therefore, it seems that, in order to explain the experimental results of the femto-techniques, it will be necessary to complement the existing chemical reactivity theories with electronic density descriptors of the events that take place in the vicinity of the

* Corresponding author. E-mail: esquivel@xanum.uam.mx.
[†] Universidad Autónoma Metropolitana-Iztapalapa.
[‡] Departamento de Física, Universidad de Granada.
[||] Instituto Carlos I de Física Teórica y Computacional, Universidad de Granada.
[§] Universidad de Zaragoza.
[⊥] University of Hyderabad.

10.1021/jp908898w
Published on Web 01/05/2010

TS region, wherein the chemical bonds are actually being formed or destroyed.

In connection with the above, there are a number of studies in the literature which have employed density descriptors to study either the TS structure or to follow the course of the chemical reaction path. For instance, Shi and Boyd[9] performed a systematic analysis of model S_N2 reactions in order to study the TS charge distribution in connection with the Hammond−Leffler postulate. Bader et al. developed a theory of reactivity based solely on the properties of the charge density by employing the properties of the Laplacian of the density, so as to align the local charge concentrations with regions of charge depletion of the reactants by mixing in the lowest-energy excited state of the combined system to produce a relaxed charge distribution corresponding to the transition density.[10] By studying the time evolution of a bimolecular exchange reaction, Balakrishnan et al. showed that information-theoretic entropies in dual or phase space rises to a maximum in a dynamical study.[11] Following the course of two elementary S_N2 reactions, Ho et al. showed that information-theoretic measures were able to reveal geometrical changes of the density which were not present in the energy profile although the TS was not apparent from the study.[12] In an attempt to build a density-based theory of chemical reactivity, Knoerr et al.[13] reported correlations between features of the quantum-mechanically determined charge density and the energy-based measures of Shaik and collaborators to describe the charge transfer, stability, and charge localization accompanying an S_N2 reaction.[14] Moreover, Tachibana[15] was able to visualize the formation of a chemical bond of selected model reactions by using the kinetic energy density $n_T(\mathbf{r})$ to identify the intrinsic shape of the reactants, the TS, and the reaction products along the course of the IRC. The reaction force of a system's potential energy along the reaction coordinate has been employed to characterize changes in the structural and/or electronic properties in chemical reactions.[16]

In recent years, there has been an increasing interest in applying information-theory (IT) measures to the electronic structure of atoms and molecules;[17] however, it has not been clearly assessed whether information-theoretic measures are good descriptors for characterizing chemical reaction parameters, that is, the stationary points of the IRC path (the TS and the equilibrium geometries of the complexes species) and the bond breaking/forming regions. Recently, significant advances have been achieved with information-theoretic analyses which allow a phenomenological description of the course of two elementary chemical reactions by revealing important chemical regions that are not present in the energy profile such as the ones in which bond forming and bond breaking occur.[18a] Furthermore, the synchronous reaction mechanism of a S_N2 type chemical reaction and the nonsynchronous mechanistic behavior of the simplest hydrogen-abstraction reaction were predicted by use of Shannon-entropies analysis.[18b]

Experimental and theoretical evidence have recognized the importance of sylilene, SiH_2, in silicon -hydride chemistry. This molecule is an important reactive intermediate in the thermal[19] and photochemical decomposition[20] of silicon hydrides such as silane and disilane. Besides, the reactions of silylene are also of interest because they serve as a model for gas-phase acid/base chemistry. For instance, silylene insertion reactions, $SiH_2 + H-Y$, have produced a significant amount of experimental[21] and theoretical[22] data. The insertion reactions of silylene have been considered as test systems for comparison of the accuracy of various levels of quantum-chemical calculations against kinetic and thermochemical data.[23]

The purpose of the present study is to follow the IRC path of the simplest silylene insertion reaction, $SiH_2 + H_2$, to unveil those elementary transformations which may provide with additional insight into the chemical characterization of a three-center insertion reaction. The motivation for the study is threefold: (i) the recent advances on Shannon-entropies analysis in predicting chemical processes which are largely invisible for the standard energetic ones,[18] (ii) the inherent difficulties that this type of reactions pose of being highly unsymmetrical and with very low-energy barriers, and (iii) to provide with a information-theoretic characterization for the two-step electrophilic−nucleophilic mechanism proposed for the silylene insertion reaction. The above will be attempted by use of Shannon entropies in position and momentum spaces calculated from molecular densities at the IRC obtained at high levels of theory. In order to characterize the critical points of the entropies, several charge density descriptors will be employed, such as the molecular electrostatic potential (MEP), multipole analysis (DMA), atomic electric potentials and charges fitted to the MEP, dipole moments, geometrical parameters and reactivity parameters of conceptual density functional theory (DFT), such as the hardness and the softness.

Theoretical Details

Throughout the study, we will employ Shannon information entropies in conjugated spaces, along with several physical descriptors commonly used in theoretical chemistry, which will be defined in this section.

The information-theoretic quantities under study are the Shannon entropies in position and momentum spaces[24] defined as

$$S_r = -\int \rho(\mathbf{r}) \ln \rho(\mathbf{r})\, \mathrm{d}^3\mathbf{r} \tag{1}$$

and

$$S_p = -\int \gamma(\mathbf{p}) \ln \gamma(\mathbf{p})\, \mathrm{d}^3\mathbf{p} \tag{2}$$

respectively, where $\rho(\mathbf{r})$ and $\gamma(\mathbf{p})$ denote the molecular electron density distributions in the position and momentum spaces, each duly normalized to unity. The Shannon entropy in position space S_r behaves like a measure of delocalization or lack of structure of the electronic density in the position space, and hence, S_r is maximal when knowledge of $\rho(\mathbf{r})$ is minimal. The Shannon entropy in momentum space S_p is largest for systems with electrons of higher speed and is smaller for relaxed systems where kinetic energy is low. Entropy in momentum space S_p is closely related to S_r by the uncertainty relation of Bialynicki-Birula and Mycielski,[25] which shows that the entropy sum $S_T = S_r + S_p$ is a balanced measure and cannot decrease arbitrarily. For one-electron atomic systems, it may be interpreted as follows: the localization of the electron's position results in an increase of the kinetic energy and a delocalization of the momentum density, and conversely.

The MEP represents the molecular potential energy of a proton at a particular location near a molecule,[26] at nucleus A for example. Then, the electrostatic potential, V_A, is defined as

$$V_A = \left(\frac{\partial E^{\text{molecule}}}{\partial Z_A}\right)_{N,Z_{B\neq A}} = \sum_{B\neq A} \frac{Z_B}{|R_B - R_A|} - \int \frac{\rho(\mathbf{r})\, \mathrm{d}r}{|\mathbf{r} - R_A|} \tag{3}$$

where $\rho(\mathbf{r})$ is the molecular electronic distribution and Z_A is the nuclear charge on atom A, located at R_A. Generally speaking, a negative electrostatic potential corresponds to the attraction of the proton by the concentrated electron density in the molecules from lone pairs, pi-bonds, and so forth (colored in shades of red in standard contour diagrams). A positive electrostatic potential corresponds to repulsion of the proton by the atomic nuclei in regions where low electron density exists and the nuclear charge is incompletely shielded (colored in shades of blue in standard contour diagrams).

The most popular methods for extracting charges from molecular wave functions are based on fitting of the atomic charges to the MEP computed with ab initio methods. The charge fitting procedure consists of minimizing the root-mean squared deviation between the coulombic potential generated by the atomic charges and the MEP. These nonbonded electric (atomic) potentials (EP) along with the fitted atomic charges (q_i) will be employed throughout the study by use of the CHELPG method.[27]

By employing a proper partitioning scheme for the charge density, one can place centers throughout the molecule so that the charge density can be analyzed in their vicinity. Thus, the charge distribution around the centers gives rise to multipoles at those centers, that is, an overall charge at the center, a dipole, a quadrupole, and so forth. A multipole expansion can then be used to predict the electrostatic potential at any location in space, and the methodology to achieve this is called the DMA,[28] which we have also employed for our chemical reaction study.

We have also evaluated some reactivity parameters that may be useful to analyze the chemical reactivity of the processes. Parr and Pearson proposed a quantitative definition of hardness (η) within conceptual DFT:[29]

$$\eta = \frac{1}{2S} = \frac{1}{2}\left(\frac{\partial \mu}{\partial N}\right)_{v(\mathbf{r})} \tag{4}$$

where $\mu = ((\partial E)/(\partial N))_{v(\mathbf{r})}$ is the electronic chemical potential of an N-electron system in the presence of an external potential $v(\mathbf{r})$, E is the total energy, and S is called the softness within the context of DFT. By using the finite difference approximation, eq 4 would be

$$\eta = \frac{1}{2S} \approx (E_{N+1} - 2E_N + E_{N-1})/2 = (I - A)/2 \tag{5}$$

where E_N, E_{N-1}, and E_{N+1} are the energies of the neutral, cationic, and anionic systems, respectively and I and A are the ionization potential (IP) and electron affinity (EA), respectively. Applying Koopmans' theorem,[30] eq 4 can be written as:

$$\eta = \frac{1}{2S} \approx \frac{\varepsilon_{\mathrm{LUMO}} - \varepsilon_{\mathrm{HOMO}}}{2} \tag{6}$$

where ε denotes the frontier molecular orbital energies. It is worth mentioning that the factor 1/2 in eqs 4−6 was put originally to make eq 4 symmetrical with $\mu = ((\partial E)/(\partial N))_{v(\mathbf{r})} = (I + A)/2$, although it has been recently disowned.[31] In general terms, hardness and softness are good descriptors of chemical reactivity; the former measures the global stability of the molecule (larger values of η means less reactive molecules), whereas the S index quantifies the polarizability of the molecule.[32] Thus, soft molecules are more polarizable and possess predisposition to acquire additional electronic charge.[33] The chemical hardness η is a central quantity for use in the study of reactivity and stability, through the hard and soft acids and bases principle.[34] A comprehensive review on hardness has been recently published by Ayers.[35]

Results and Discussion

The electronic-structure calculations performed in the present study were carried out with the Gaussian 03 suite of programs.[36] The geometrical parameters for the TS were calculated by means of the synchronous transit-guided quasi-Newton (STQN) method at the MP2/6-31G(d,p) level followed by a vibrational-frequency calculation to verify the existence of the saddle point of the first order; this was done at the same level of theory through the second derivatives of the energy calculated analytically. Then, the intrinsic reaction path for the three-center insertion reaction $SiH_2 + H_2 \rightarrow SiH_4$ was obtained at two different levels of theory, the MP2/6-31G(d,p) and the CISD/6-311++G(d,p) ones, which produced an IRC path (IRCP) of 72 and 53 points, respectively, evenly distributed among the IRCP. Then, a higher level of theory and a well-balanced basis set (with diffuse and polarized functions) were chosen for determining all the properties for the chemical structures corresponding to the IRCP. Thus, the QCISD(T) method will be employed in addition to the 6-311++G(d,p) basis set, unless otherwise stated. The hardness and softness chemical parameters were calculated by use of eq 6, and the standard hybrid B3LYP functional. Molecular frequencies corresponding to the normal modes of vibration depend on the second derivatives of the energy (Hessian matrix) at the nuclei positions of the stationary points. The eigenvalues of the Hessian for the normal mode associated with the TS (possessing an imaginary frequency) were determined analytically for all points of the IRC path at the MP2 level of theory. The molecular information entropies in position and momentum spaces for the IRC path were obtained by employing software developed in our laboratory along with 3D numerical integration routines[37] and the DGRID suite of programs.[38] The bond breaking/forming regions along with electrophilic/nucleophilic atomic regions were calculated through the MEP and DMA analyses by use of MOLDEN.[39]

It has been proposed[40] that the silylene insertion reaction into hydrogen occurs in two stages: a three-center bond is formed through the electrophilic attack from the silylene to the H—H molecule followed by a nucleophilic interaction from the H—H to the silylene. In molecular orbital terminology, the electrophilic step is due to the interaction of the unoccupied π^*-type p orbital on the Si of silylene with the σ H—H orbital followed by a the nucleophilic step corresponding to the interaction between the occupied σ -type lone pair (lp) of silylene and the H—H σ^* antibonding molecular orbital.[22] One of the goals of the present study is to verify the elctrophilic/nucleophilic stages of the reaction through the phenomenological description of the IRCP for the silylene insertion reaction into the hydrogen molecule (SIRH).

Because a significant number of theoretical studies have been devoted to insertion reactions of silylene,[22,23,41] we found it useful to take advantage of the experience gained through these studies in order to choose a good methodology and basis set which could describe properly all the observed features of the SIRH at low computational cost. These can be summarized as follows: (i) the calculated barrier heights are generally found to be in good agreement with the experimental value[42] of 1 kJ/mol as larger basis are employed and correlation is included and (ii) a loose cluster (prereaction complex) with a shallow minimum

TABLE 1: Total Energies (E), Barrier Heights (ΔE), and Geometrical Parameters of the PRC and the TS Calculated from Different Methods: MP2/6-31(d,p) (First Row), CISD/6-311++G(d,p) (Second Row), QCISD/6-311G(d,p) from ref 23 (Third Row), and B3LYP/6-311++G(3df,2pd) from ref 23 (Forth Row)[a]

E	ΔE[b]	R(Si−H1)	R(Si−H3)	R(Si−H4)	R(H3−H4)	A(H1−Si−H2)
			Stationary Point: PRC			
−291.247	−15	1.501	1.895	1.811	0.777	96
−291.304	−6	1.506	1.935	1.865	0.779	95
−291.351	−28	1.509	1.936	1.859	0.783	95
−291.836	−32	1.513	1.870	1.778	0.805	95
			Stationary Point:TS			
−281.233	20	1.484	1.685	1.543	1.107	113
−291.289	32	1.479	1.669	1.524	1.163	113
−291.340	−1	1.479	1.661	1.522	1.117	110
−291.827	−7	1.484	1.647	1.522	1.140	110

[a] Total energies in hartrees, barrier heights in kJ/mol, distances in angstroms, and angles in degrees. [b] $\Delta E = E(\mathrm{S}) - E(\mathrm{reactants})$ where S stands for PRC or TS. E(reactans) in Hartrees: SiH_2(MP2), −290.0834; SiH_2(CISD), −290.1331; H_2(MP2), −1.1576; H_2(CISD), −1.1684.

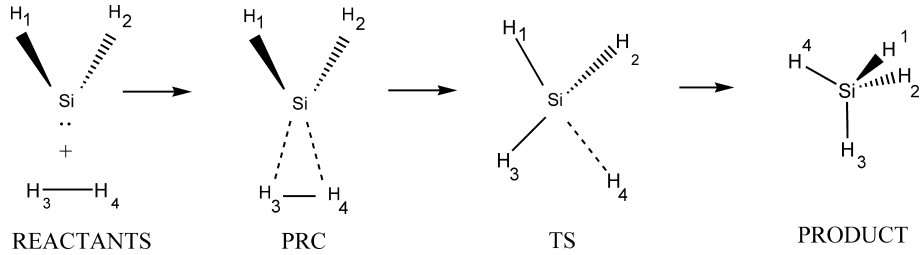

Figure 1. Stationary points of the PES along the Silylene insertion reaction into H_2 corresponding with the prereaction complex (PRC), the TS structure, and the product.

has been reported to exist along the reaction path toward the reactants region.[22,23] Because it has been reported that the MP2/6-31G(d,p) methodology predicts the Si−X bond lengths in good agreement with experiment and possesses the above-mentioned features, we have chosen this combination of theory and basis set in order to generate the TS structure and calculate the IRC to analyze the chemical phenomena that molecules exert along the course of the SIRH. Once the IRCP is generated, all the chemical structures (72 for the IRCP at the MP2 level) are recalculated at the QCISD(T) level of theory in a basis-set that includes polarized as well as diffuse functions. This choice permits to report physical/chemical descriptors at a higher level of theory but within the chemical frame (IRCP) that provides the well studied MP2/6-31G(d,P) methodology as we mentioned before. The whole computational strategy is represented at the QCISD(T)/6-311++G(d,p)//MP2/6-31G(d,p) method.

In Table 1, we have reported some of the geometrical parameters which characterize those structures in the stationary points of the PES, that is, the prereactive complex (PRC) and the TS. Selected values reported in the literature are also included for comparison purposes. The atom numbering corresponds to that of Figure 1. The comparison of the geometrical values reported in Table 1 shows a very good agreement for the different methodologies. Values for the energy values and barrier heights seem to be more dependent on the choice of the method and basis set. For the purposes of our study, we may anticipate that it is not necessary to perform state-of-the-art calculations with regard to electron correlation because we are not focused in obtaining accurate energy values but in making a phenomenological description of the reaction in a qualitative manner.

The corresponding energy profile calculated at the QCISD(T)/6-311++G(d,p)//MP2/6-31G(d,p) level for the IRC of the SIRH is depicted in Figure 2 along with the entropy sum ($S_r + S_p$) obtained from eqs 1 and 2, and the conjugated Shannon entropies in position and momentum spaces are depicted in Figure 3. It

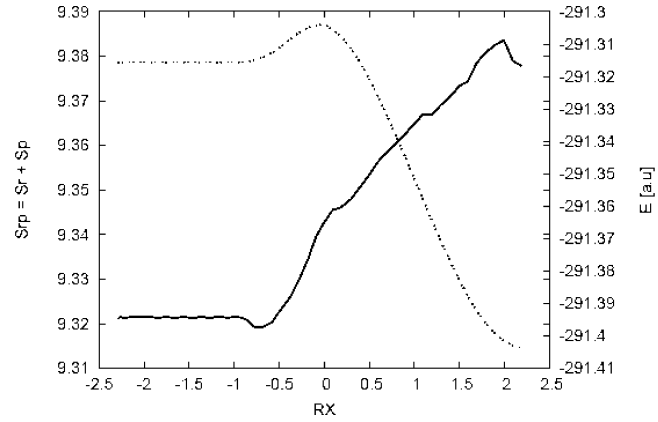

Figure 2. Total energy values (dashed line) in Hartrees and the Shannon entropy sum (solid line) for the IRCP of $SiH_2 + H_2 \rightarrow SiH_4$ at the QCISD(T)/6-311++G//MP2/6-31G(d,p) level.

is worth mentioning that we have performed similar TS and IRC calculations at the CISD/6-311++G(d,p) level in order to assess the reliability of our observations by determining whether the new TS (geometrical parameters reported in Table 1) and the corresponding IRCP may cause a significant change in the entropies; we observe no significant differences in the shape of the profiles though, other than a slight change in the quantitative values for the entropies.

The general observation that we may note from Figure 2 is that the energy and the entropy behave in an opposite way, which is expected from a information-theoretic perspective; that is, as IRC approaches the chemical structure associated with the product, the energy approaches a minimum, whereas the entropy tends to a maximum—which corresponds to a highly delocalized electronic distribution in the conjugated phase space. Besides, both measures indicate the expected zones that we mentioned before; that is, the more evident one is the TS at around $R_X \approx 0$, which is characterized by the energy maximum

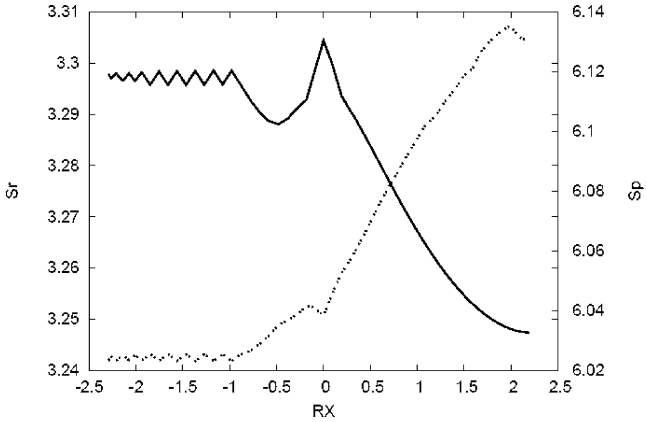

Figure 3. Shannon entropies in position (solid line) and momentum (dashed line) spaces for the IRP of $SiH_2 + H_2 \rightarrow SiH_4$ QCISD(T)/6-311++G(d,p)

and also by a noticeable inflection point in the entropy sum. Furthermore, at the left side of the TS, the prereaction complex is predicted in an similar way by both the energy and the entropy sum. This is more evident by inspection of the PRC energy barriers reported in Table 1, which are negative; that is, the total energy for the reactants ($SiH_2 + H_2$) is above the energies for both the PRC and the TS (the corresponding entropies for the reactants are not reported, but they are below the ones for the PRC and the TS). Therefore, the flat region at the beginning of the IRCP corresponds to a local minimum for the energy and a local maximum for the entropy sum. The region at the right of the TS is also predicted by both quantities as we discussed above in connection with its general behavior. However, it is worth noting that aside of the global regions, the entropy sum shows much more structure locally, which might be associated with other chemical complexes and/or physical processes not yet predicted on energetic grounds. This will be discussed below in connection with the entropies in each conjugated space and by use of several physical descriptors of the density.

Shannon entropies in position and momentum spaces behave in opposite ways and show interesting profiles as it may be observed from Figure 3. The general feature that we may note is the close resemblance between the entropy sum in Figure 2 and the one in momentum space which seems to be characterized in a similar way, except for the fact that it is now possible to link a physical energetic (kinetic) behavior along the course of the IRCP; that is, as the reaction progresses, the kinetic energy increases up to a point where the reaction product is reached. However, it is interesting to note that several features for the S_p measure along the IRCP are readily apparent: (i) the entropy values oscillate at the region where the PRC predominates, (ii) there is a local maximum at the TS vicinity, around $R_X \approx -0.3$, (iii) there is a local minimum associated to the TS, (iv) an inflection point is found at $R_X \approx +1.0$, and (v) thre is a local maximum at the end of the IRCP.

On the side of the position-space entropy, we also find much structure in all regions of the IRCP, and overall, as the reaction progresses, the entropy tends to decrease, indicating a very localized position density associated with the product which we interpret as a highly stable chemical structure as compared with the rest on the IRCP. As for the local behavior for the S_r, we notice an overall opposite behavior as compared with that of the momentum entropy. Again, several features can be noticed from the S_r profile: (i) an oscillating behavior at the PRC region, (ii) a pronounced minimum at the close vicinity of the TS, around $R_X \approx -0.5$, (iii) an inflection point before the TS at $R_X \approx -0.3$, (iv) a local maximum associated with the TS, and (v) an inflection point after the TS at $R_X \approx -0.3$. The obvious question to ask is whether the above features for the S_r and S_p are linked to physical processes or they are mere artifacts of the electronic-structure calculations. In order to provide reasonable answers to this, we will resort to a series of physical descriptors discussed below, although it is useful to mention at this point that similar features are observed at the two different levels of theory, MP2 or CISD, as mentioned above. The physical interpretation associated with the information-theoretic analysis of the conjugated entropies and their local features aforementioned will be provided later, as soon as we establish some links with chemical concepts and physical processes.

We will proceed to describe the course of the SIRH reaction based on the findings of previous work published by several auhors.[22,23,40,43] Accordingly, the reaction proceeds as follows (numbering of Figure 1).

Stage I: as the hydrogen molecule approaches the silylene molecule (reactants in Figure 1), a three-center interaction takes place through the electrophilic attack from the silylene (π^*-type p MO) to the H_3—H_4 (σ bonding MO) molecule and the PRC complex is formed (see Figure 1), which is energetically stable through a chemical structure which depicts (see Table 1) a more favorable interaction with one of the hydrogen atoms, H_3 in this case, as the other one (H_4) is getting loose because of its repulsive interaction with the internal hydrogens in the silylene molecule.

Stage II: as the reaction proceeds, a competition to form the new bond (Si—H_3) is established between the three centers. This competitive interaction causes strong vibrational effects among all the centers, which is reflected through an oscillatory behavior of the interactomic distances and the internal angle (H_1—Si—H_2) at $-2.3 < R_X < -1.0$.

Stage III: at the end of the last stage, ($R_X \approx 1.0$), the new bond starts forming, and the R(Si—H_3) distance gets shorten while the bond breaking process of the H_2 molecule begins. At the end of this stage ($R_X \approx -0.5$), the Si—H_3 bond-forming process has been completed while the bond-cleavage process

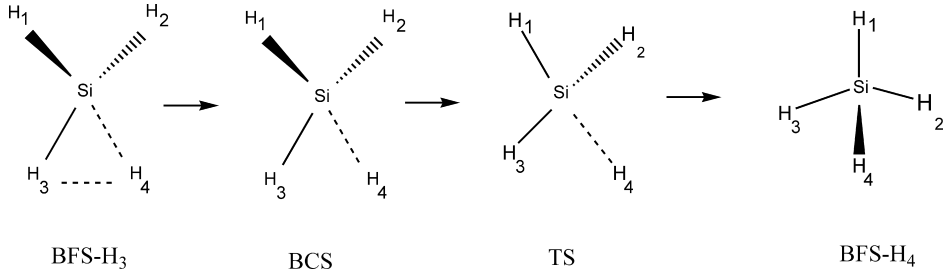

Figure 4. Density-based structures BFS-H_3, BFS-H_4, and BCS for the SIRH.

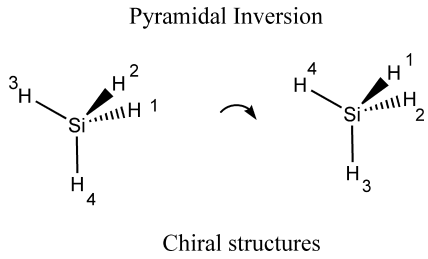

Figure 5. Pyramidal inversion at the end of the IRCP for the SIRH.

gets finished. Bond-forming and bond-cleavage structures (BCS and BFS, respectively) are linked to the process (see Figure 4).

Stage IV: as the internal dihedral angle (H_3−Si-H_2−H_1) gets larger the TS structure (Figure 1) is reached (Rx = 0) at the expense of increasing the electrostatic interactions by relaxing the structure and delocalizing its corresponding electronic distribution.

Stage V: as the reaction progresses, within $0 < R_X < +1$, the nucleophilic interaction from the remaining H_3−H_4 molecule (σ^* antibonding MO) to the silylene (σ-type lp MO) causes the increase of the internal angles H_1−Si−H_2 and H_3−Si−H_2−H_1 while a trigonal pyramid is formed with the H_4 atom at the apex and the rest of the hydrogen atoms at the corners of the trigonal base (C_s to C_{3v} transformation). At $R_X \approx +1$, the dihedral angle reaches its maximum distortion (180°), and the internal system (H_3−Si−H_2−H_1) turns into a planar structure; this is when the second bond between the Si and the H_4 atoms is formed. Hence, a BFS is linked to the process (see Figure 4).

Stage VI: At $R_X > +1$, the dihedral angle becomes negative and gets shorten in such a way that hydrogens in the trigonal base flip like an inverting umbrella to an alternative identical structure by causing a change in chirality. At the final course of the SIRH ($R_X \approx +2$), the new molecule (SiH_4) reaches its typical tetrahedral geometry. However, troughout the course of the reaction, the molecule built up such an amount of kinetic energy (KE) that, in order to become energetically stable, the accumulated KE gets liberated at the ending stage of the IRCP, and then, a pyramidal inversion of the tetrahedron occurs (see Figure 5).

The first part of the hypothesis considers a phenomenological description of the SIRH based on density-based criteria by incorporating new BFSs (BFS-H_3 and BFS-H_4) and a BCS into the sequence of energy-based structures to fully explain the course of the reaction. This proposal is represented in Figure 4 and is supported by evidence obtained from several sources by employing density descriptors and reactivity criteria, and this will be presented next in connection with the above-mentioned process.

Phenomenological description of SIRH according to energy and density related properties and reactivity parameters are as follows (numbering of Figure 1).

Stage I (PRC existence): this is an energy-based structure which is revealed by the PES, and its geometrical parameters are reported in Table 1 by use of several methodologies.

Stage II (three-center oscillatory behavior): this is revealed through Figures 6−10, where several geometry and density descriptors are depicted, starting at the PRC region ($R_X \approx -2.3$) up to $R_X \approx -1.0$. In Figure 6, we have plotted the bond distances for Si−H_3 and Si−H_4 along with the internal angle H_1−Si−H_2, where the oscillatory behavior is witnessed by these geometrical parameters. The oscillatory behavior is also observed at the same region through the dipole moment (Figure 7), the atomic charges

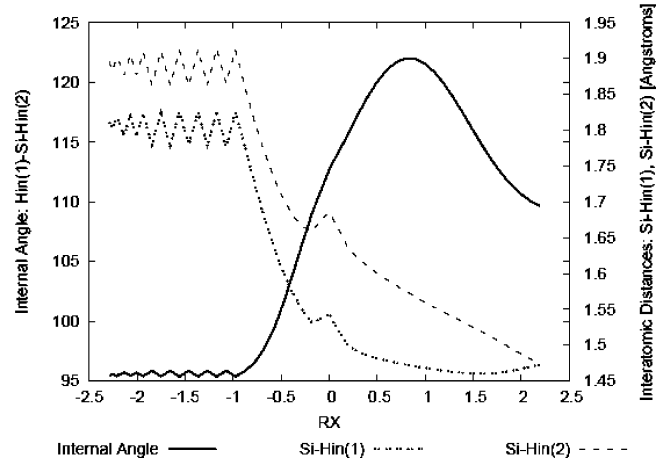

Figure 6. Internal angle H_1−Si−H_2 (solid line) in degrees and bond distances R_2(Si−H_3) (dotted line) and R_1(Si−H_4) (dashed line) in angstroms for the SIRH at the QCISD(T)6-311++G//MP2/6-31G(d,p) level.

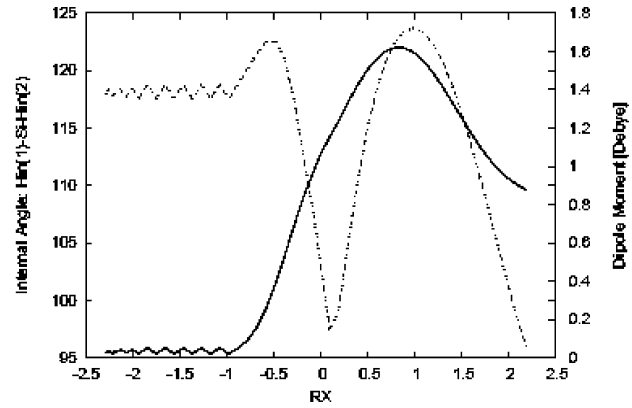

Figure 7. Internal angle H1−Si−H2 (solid line) in degrees and dipole moment (dashed line) in debyes for the SIRH at the QCISD(T)6-311++G//MP2/6-31G(d,p) level.

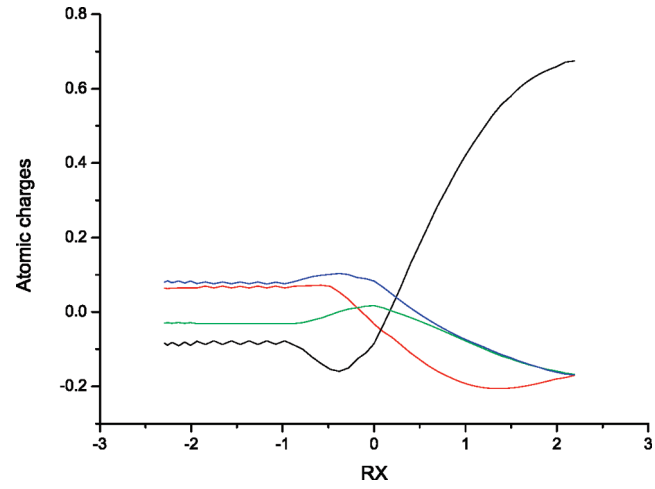

Figure 8. Atomic charges for the Si (black), H_1/H_2 (green), H_3 (blue), H_4 (red) atoms for the SIRH at the QCISD(T)6-311++G//MP2/6-31G(d,p) level.

(Figure 8), the atomic electric potentials of the hydrogen atoms (Figure 9), and for the silicon atom (Figure 10).

Stage III (bond forming Si−H_3 and bond-cleavage H_3−H_4 regions): at the end of the last stage ($R_X \approx -1.0$), the Si−H_3 bond starts forming, and the H_3−H_4 bond starts breaking; this is witnessed by several descriptors. For instance, the internal

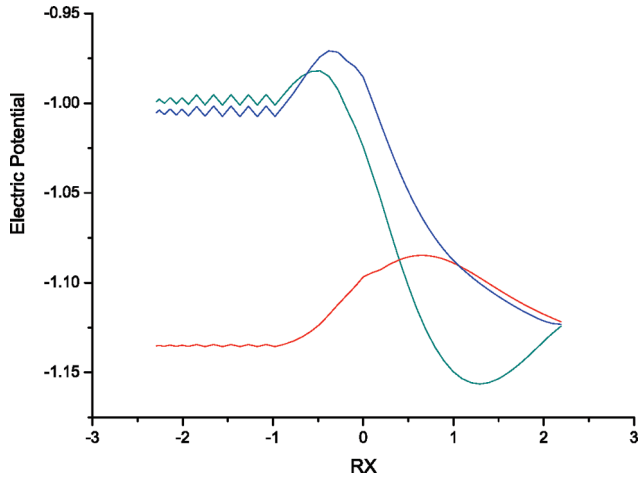

Figure 9. Electric atomic potentials fitted from the MEP for the H_1/H_2 atom (red), H_3 (blue), and H_4 (green) for the SIRH at the QCISD(T)6-311++G//MP2/6-31G(d,p) level.

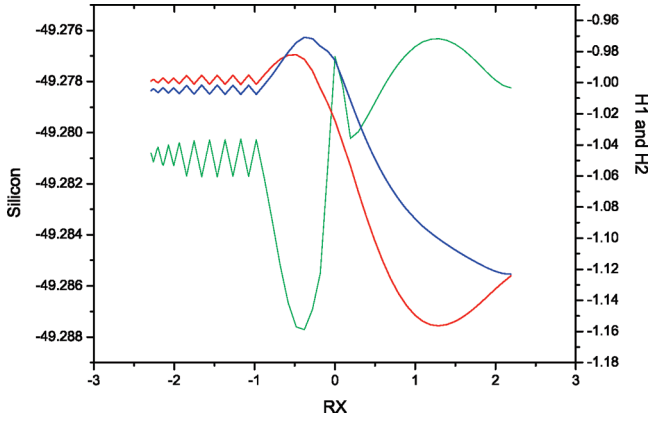

Figure 10. Electric atomic potentials fitted from the MEP for Si atom (green), H_3 (blue), and H_4 (red) for the SIRH at the QCISD(T)6-311++G//MP2/6-31G(d,p) level.

angle starts increasing rapidly at $R_X \approx -1.0$ (Figure 6), and the dipole moment increases at the same region and reaches a maximum at $R_X \approx -0.5$ where the Si—H_3 bond gets formed and the H_3—H_4 gets broken, which means that the corresponding BFS-H_3 is highly polarized and hence chemically reactive as compared with the molecules at its vicinity. This is in agreement with the atomic charges, depicted in Figure 8, which increase positively for the hydrogen atoms, whereas for the silicon atom, one increases negatively at $R_X \approx -1.0$. Both are showing maxima and minima, respectively, at $R_X \approx -0.5$, where the bond-forming and bond-breaking is completed; that is, at this region, the atoms get their maximum polarization. Another descriptor that proves these regions is the atomic electric potential (PE), depicted for the hydrogen atoms in Figure 9 and for the silicon atom in Figure 10. At $R_X \approx -1.0$, the PE of the hydrogen atoms increases (negatively), and for the silicon atom, it decreases (negatively), indicating that the bond forming/breaking process has initiated up to a critical point where all the PE values are extremum, exactly at the region where the processes get completed, at $R_X \approx -0.5$. Again, the PE behavior is in agreement with the other descriptors in that at the region of highest polarization, the electric potential difference (maximum to minimum) is the largest; that is, whereas for the Si atom its capacity to acquire charge is minimal (with an atomic negative charge being maximal, see Figure 8), the capacity of the H_3 atom to acquire charge is maximal (with an atomic negative charge being minimal). This electrostatic situation marks the end of the bond rupture and the bond forming and indicates the existence of the bounded complex BFS-H_3 and the BCS that, in this case, coincide in the same structure because this chemical step is concerted.

Therefore, we will assigne the BFS and the BCS at the maximum potential difference. In Figures 11 and 12, we present contour diagrams for the DMA analysis through sequences of selected frames, to show the MEP regions through a multipole expansion. Again, the bond-forming process at onset of the $R_X \approx -1.0$ region is clearly shown in Figure 11 through the electrophilic/nucleophilic regions to mimic the bonding process pictorically. Furthermore, the bond-breaking process is vividly represented in Figure 12 through a selected sequence of MEP frames at the onset of the $R_X \approx -0.5$ region.

Stage IV (TS region): this is an energy-based critical point which is obtained through the PES, and their geometrical data are reported in Table 1 for several methods. Its existence is clearly predicted by some density descriptors through extremum values (Figures 6, 7, and 10). For instance, the bond distances for the Si—H atoms (Figure 6) clearly show maxima at $R_X = 0$, and the dipole moment (Figure 7) shows a minimum value, whereas the PE of the silicon atom (Figure 10) shows a local minimum. That is, the dipole moment of TS structure is almost null, which means that the TS is locally stable, not chemically reactive, and with a not-polarizable electron density, corresponding to a highly localized structure. At this point, the PE of Si reaches a maximum, that is, maximal capacity to lose or to acquire charge, and this is in agreement with its atomic charge at $R_X = 0$ (see Figure 8), wherein it is almost neutral.

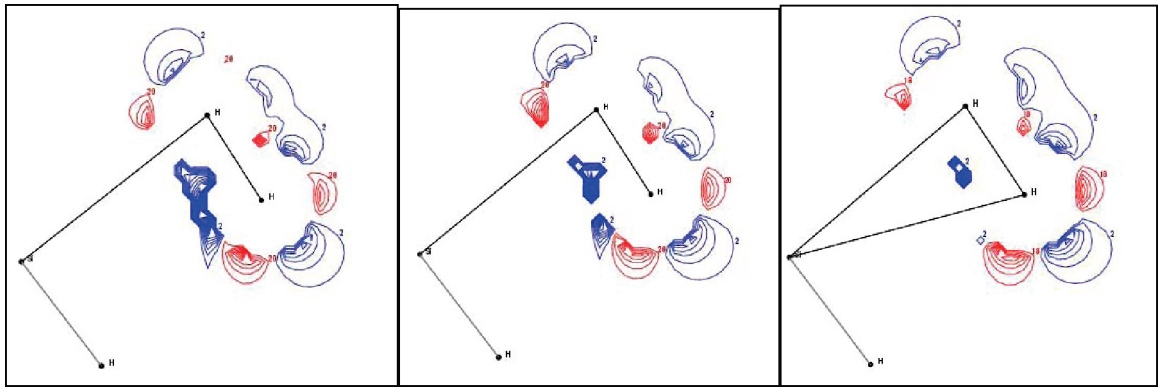

Figure 11. Sequence of DMA images showing the bond forming of Si—H_3 at the vicinity of $R_X \approx -1.0$. Blue contour lines depict nucleophilic regions, and red contour lines depict electrophilic regions. DMA calculations for the SIRH at the QCISD(T)6-311++G//MP2/6-31G(d,p) level.

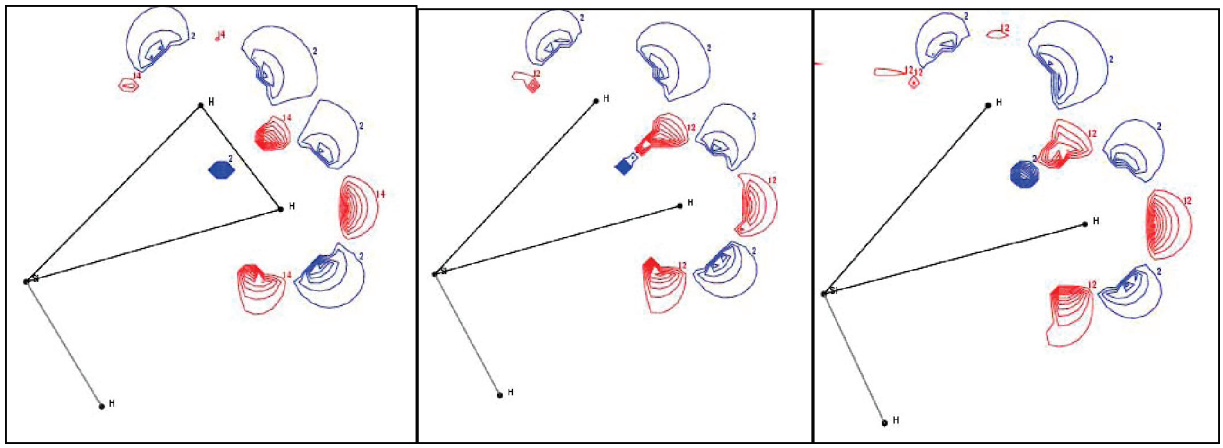

Figure 12. Sequence of DMA images showing the bond cleavage of H_3—H_4 at the vicinity of $R_X \approx -0.5$. Blue contour lines depict nucleophilic regions, and red contour lines depict electrophilic regions. DMA calculations for the SIRH at the QCISD(T)6-311++G//MP2/6-31G(d,p) level.

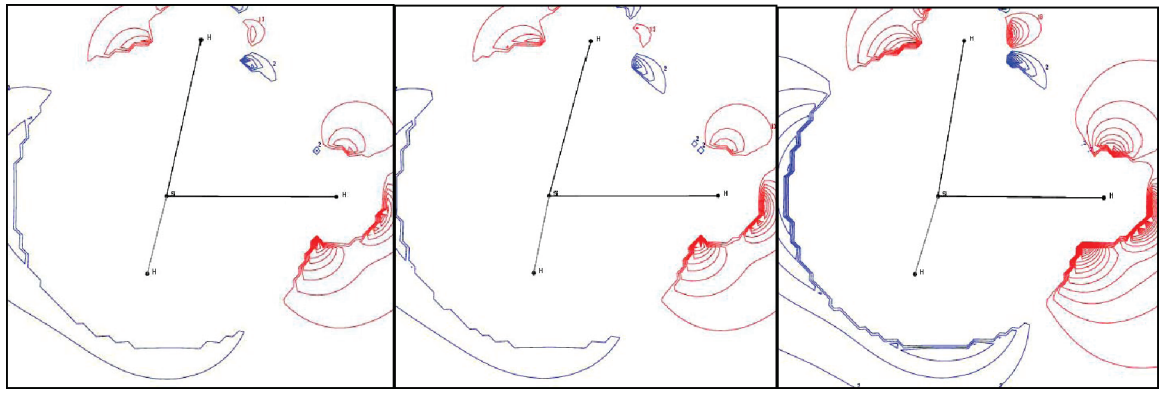

Figure 13. Sequence of DMA images showing the bond forming of Si—H_4 (at the top of the frames) and the nucleophilic interaction from the H_3—H_4 to the SiH_2 at the vicinity of $R_X = +1$. Blue contour lines depict nucleophilic regions, and red contour lines depict electrophilic regions. DMA calculations for the SIRH at the QCISD(T)6-311++G//MP2/6-31G(d,p) level.

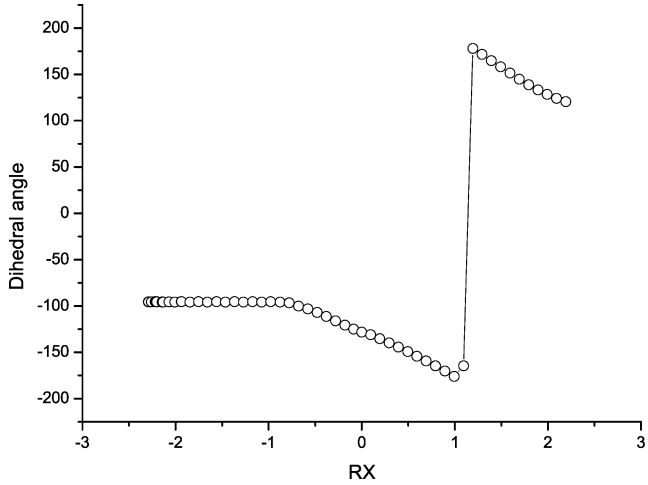

Figure 14. Dihedral H_3—Si—H_2—H_1 angle in degrees for the SIRH at the QCISD(T)6-311++G//MP2/6-31G(d,p) level. 14

Stage V (bond-forming Si—H_4 region): as the reaction progresses, within $0 < R_X < +1.1$, the nucleophilic interaction from the H_3 and H_4 atoms to the silylene causes the increase of the internal angles H_1—Si—H_2 and H_3—Si—H_2—H_1 so as to become a trigonal pyramid. At $R_X \approx +1.1$, the dihedral angle reaches its maximum distortion (180°), and the internal system (H_3—Si—H_2—H_1) turns into a planar structure; this is when the second bond between Si and the H_4 atom is formed. This process is witnessed by several descriptors, for instance, the internal angle H_1—Si—H_2 in Figure 6 which reaches a maximum at a region close to $R_X \approx +1.1$. At this point, the bond forming of Si—H_4 is completed, and several descriptors clearly suggest the existence of the BFS. Again, the dipole moment shows a maximum at $R_X \approx +1.1$, meaning that this structure is highly polarized and hence chemically reactive. The PE atomic values indicate clearly the completion of the BFS by a maximal potential difference; that is, whereas the Si atom shows a maximum PE, the H_4 atoms show a minimum, meaning a high capacity for the Si atom to acquire charge, and this is indeed the case because its atomic charge (Figure 8) tends to increase positively, whereas the H_4 atoms possess a minimal capacity to acquire charge because their atomic charge is already at its maximum extent (minimum in Figure 8). Again, this electrostatic situation marks the end of the bonding process and indicates the existence of a complete bounded complex, the BFS-H_4. Therefore, we will assign the BFS and the BCS at the maximum potential difference. Finally, in Figure 13, we show contour diagrams for the DMA analysis through sequences of selected frames for the MEP regions through a multipole expansion. Again, the bond-forming process at onset of the $R_X \approx +1$ region is clearly shown through the electrophilic/nucleophilic regions to mimic the bonding process pictorically. As the bond is formed, the charge transfer from the Si atom to the hydrogens H_4 and H_3 is clearly shown through the nucleophilic regions for Si (blue contour lines) and the electrophilic ones for H_4 and H_3 (red contour lines). This is in agreement with the atomic charges (Figure 8) and the atomic PE (Figures 9 and 10), thus corroborating the nucleophilic (to silicon) step of the reaction.

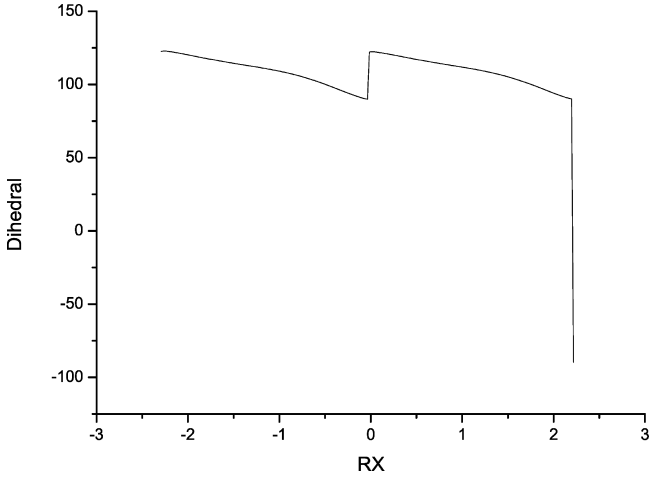

Figure 15. Dihedral X_1—X_2—Si—H_4 angle in degrees for the SIRH at the QCISD(T)6-311++G//MP2/6-31G(d,p) level. X_1 and X_2 stand for dummy atoms the X_1—X_2—Si angle of which is zero and form a perpendicular plane with the plane of the H_3 and H_4 atoms.

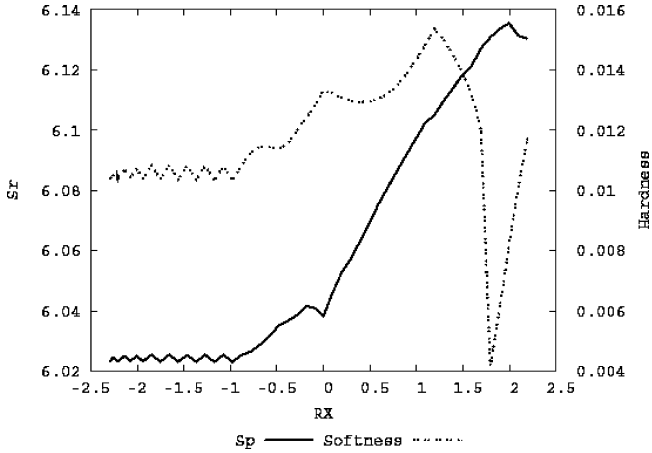

Figure 16. Shannon entropy in momentum space (solid line) and hardness values (dashed line) in a.u. for the SIRH at the MP2/6-31G(d,p)//B3LYP/6-311G level.

Stage VI (umbrella and pyramidal inversion at a chiral center): at $R_X > +1$, the dihedral angle becomes negative and gets shorten in such a way that hydrogens in the trigonal base flip like an inverting umbrella to an alternative identical structure by causing a change in chirality. This is proved by the dihedral H_3—Si—H_2—H_1 angle depicted in Figure 14 which flips at $R_X \approx +1$ clearly showing the umbrella inversion. At the final course of the SIRH ($R_X \approx +2$), the new molecule (SIH_4) reaches its typical tetrahedral geometry. However, at the ending stage of the IRCP, the accumulated KE gets liberated through a pyramidal inversion of the tetrahedron. This phenomenon is clearly shown in Figure 15 through an ad hoc dihedral angle formed by X_1—X_2—Si—H_4 where X_1 and X_2 stand for dummy atoms (see caption in Figure 15). The reactivity properties of the chemical reaction are depicted in Figure 16, through the softness values, eqs 5 and 6. From the figure, we noticed that this chemical descriptor predicts all the regions of chemical interest through local maxima at the onset of the BFS-H_3 ($R_X \approx -0.8$), at the TS and at the BFS-H_4 regions, thus associating these zones with highly polarized structures, which is in agreement with other descriptors discussed above. It is interesting to note that, at the end of the IRCP, the softness as well as the momentum entropy are able to predict the pyramidal inversion of the chiral center at $R_X \approx +2$.

The second part of the hypothesis conforms a information-theoretic phenomenological description of the SIRH based on the Shannon measures, and the proof is straightforward. According to Figures 2 and 3, we may verify that any single critical point shown in the profiles of the entropies possess a link with a physical descriptor (Figures 6−15), and hence, the conjugated Shannon entropies are able to predict the entire course of the reaction. This is relevant because we are now in the position of proposing new density(entropy)-based structures related to the bond-forming (BFS) and bond-breaking (BCS) regions. Therefore, we report in Table 2 the geometrical data for the structures BFS-H_3, BFS-H_4 and the BCS along with their energies.

Finally, in Figure 17, we have depicted the Hessian eigenvalues for the transition vector, which clearly show the saddle-point features of the TS structure and the oscillating behavior of the reactive complex as the H_2 approaches the SiH_2 molecule.

Conclusions

We have been able to assess the utility for the information-theoretic measures of the Shannon type to fully characterize the silylene insertion reaction into hydrogen. The TS structure as well as the rest of the stationary points were clearly predicted. Besides, through these chemical probes, we were capable of observing the basic chemical phenomena of bond breaking/forming showing that the Shannon measures are sensitive in detecting these chemical events. An important contribution from the present study is the prediction of new BFSs (BFS-H_3 and BFS-H_4) and the BFC which allows to fully explain the course of the reaction.

Furthermore, the TS of a reaction is commonly identified by the presence of a negative force constant for one normal vibrational mode corresponding with an imaginary frequency. However, the work of Zewail and Polanyi in TS spectroscopy has led to the concept of a reaction having a continuum of transient, a transition region rather than a single TS.[8,44] It is worth mentioning that the results of the present study show indeed the existence of such a region between the BCER before and after the TS. This is in agreement with reaction force, $F(R)$ studies,[16] where the reaction force constant, $\kappa(R)$, also reflects this continuum, showing it to be bounded by the minimum and the maximum of $F(R)$, at which $\kappa(R) = 0$.

This investigation suggests that other information-theoretic analyses should be performed in order to make a comprehensive study of the different measures. For instance, it is well-known that the Shannon entropy describes the global features of the

TABLE 2: Total Energies (E), Barrier Heights (ΔE), and Geometrical Parameters for the BFS and the BCS Calculated at the MP2/6-31(d,p) (First Row) and the CISD/6-311++G(d,p) (Second Row)[a]

density-based	E	ΔE^b	R(Si—H1)	R(Si—H3)	R(Si—H4)	R(H3—H4)	A(H1—Si—H2)
BFS-H_3/BCS	−291.240	2.6	1.482	1.681	1.572	0.89	103.9
BFS-H_4	−291.304	−165.4	1.466	1.539	1.462	1.947	118.7

[a] Total energies in aartrees, Barrier heights in kJ/mol, distances in angstroms, and angles in degrees. [b] $\Delta E = E(S) - E(\text{reactants})$ where S stands for PRC or TS. E(reactans) in hartrees: SiH_2(MP2), −290.0834; SiH_2(CISD), −290.1331; H_2(MP2), −1.1576; H_2(CISD), −1.1684.

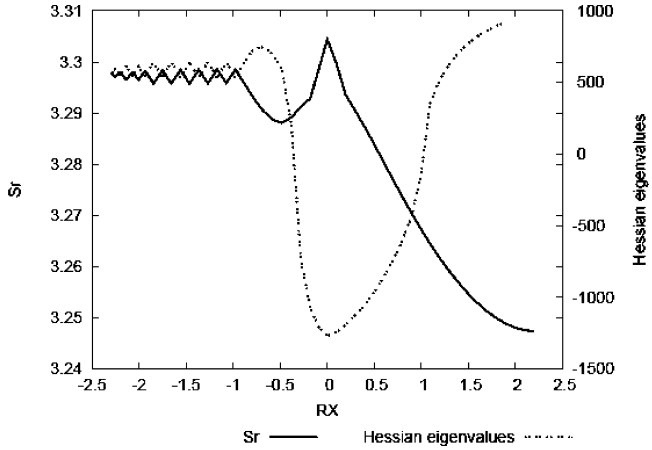

Figure 17. Shannon entropy in position space (solid line) and Hessian eigenvalues (dashed line) corresponding with the transition vector for the SIRH at the MP2/6-311++G(d,p) level in order to obtain the frequencies at the same IRC level of theory.

distribution, whereas the so-called Fisher information describes it locally.[45] This is relevant in the context of chemical reactivity. Investigations along the above-mentioned lines have been initiated in our laboratories. This type of research might be useful for people in the quest of developing a complementary conceptual theory of the chemical reactivity along the lines suggested many times by Shaik and co-workers.[46] The more chemically meaningful information about chemical processes, the more reliable and accurate the theories we can access.

Acknowledgment. We wish to thank José María Pérez-Jordá and Miroslav Kohout for kindly providing their numerical codes. R.O.E. wishes to thank Juan Carlos Angulo and Jesús Sánchez-Dehesa for their kind hospitality during his sabbatical stay on the Departamento de Física Atómica, Molecular y Nuclear at the Universidad de Granada, Spain. We acknowledge financial support through mexican Grants 08226 CONACyT and PIFI from PROMEP-SEP and spanish Grants MICINN Projects FIS-2008-02380 (J.A.), FQM-4643 and P06-FQM-2445 (J.S.D., J.C.A., and S.L.R.) of Junta de Andalucía. J.S.D., J.C.A., and S.L.R. belong to the Andalusian research group FQM-0207. Allocation of supercomputing time from the Departamento de Supercómputo at DGSCA-UNAM, the Sección de Supercomputacion at CSIRC-Universidad de Granada, and the Laboratorio de Supercómputo y Visualización at UAM is gratefully acknowledged.

References and Notes

(1) Schlegel, H. B. *Adv. Chem. Phys.* **1987**, *67*, 249.
(2) Eyring, H. *J. Chem. Phys.* **1935**, *3*, 107.
(3) Wigner, E. *Trans. Faraday Soc.* **1938**, *34*, 29.
(4) (a) Fukui, K. *Acc. Chem. Res.* **1981**, *14*, 363. (b) González, C.; Schlegel, H. B. *J. Phys. Chem.* **1990**, *94*, 5523. (c) Peng, Ch.; Schlegel, H. B. *Isr. J. Chem* **1993**, *33*, 449. (d) Peng, Ch.; Ayala, Ph. Y.; Schlegel, H. B.; Frisch, M. J. *J. Comput. Chem.* **1996**, *17*, 49. (e) Fan, L.; Ziegler, T. *J. Am. Chem. Soc.* **1992**, *114*, 10890. (f) Safi, B.; Choho, B.; Geerlings, P. *J. Phys. Chem. A* **2001**, *105*, 591. (g) Pople, J.; Krishnan, A. R.; Schlegel, H. B.; Binkley, J. S. *Int. J. Quantum Chem.* **1978**, *14*, 545. (h) González-García, N.; Pu, J.; González-Lafont, A.; Lluch, J. M.; Truhlar, D. G. *J. Chem. Theory Comput.* **2006**, *2*, 895. (i) Ishida, K.; Morokuma, K.; Komornicki, A. *J. Chem. Phys.* **1977**, *66*, 2153. (j) Schmidt, M. W.; Gordon, M. S.; Dupuis, M. *J. Am. Chem. Soc.* **1985**, *107*, 2585. (k) Baskin, C. P.; Bender, C. F.; Bauschlicher, C. W., Jr.; Schaefer, H. F., III. *J. Am. Chem. Soc.* **1974**, *96*, 2709.
(5) Shaik, S.; Ioffe, A.; Reddy, A. C.; Pross, A. *J. Am. Chem. Soc.* **1994**, *116*, 262.
(6) Shaik, S. *J. Am. Chem. Soc.* **1981**, *103*, 3692.
(7) (a) McWeeny, R. *Methods of molecular quantum mechanics*; Academic Press: London, 1989; (b) Shaik, S. In *Encyclopedia of Computational Chemistry*; Schleyer, P. v. R., Ed.; Wiley: Chichester, UK, 1998; *5*, 3143.
(8) Zewail, A. H. *Science* **1988**, *242*, 1645. Zewail, A. H. *J. Phys. Chem. A* **2000**, *104*, 5660.
(9) Shi, Z.; Boyd, R. J. *J. Am. Chem. Soc.* **1991**, *113*, 1072.
(10) Bader, R. F. W.; MacDougall, P. J. *J. Am. Chem. Soc.* **1985**, *107*, 6788.
(11) Balakrishnan, N.; Sathyamurthy, N. *Chem. Phys. Lett.* **1989**, *164*, 267.
(12) Ho, M.; Schmider; Weaver, D. F.; Smith, V. H., Jr.; Sagar, R. P.; Esquivel, R. O. *Int. J. Quantum Chem.* **2000**, *77*, 376.
(13) Knoerr, E. H.; Eberhart, M. E. *J. Phys. Chem. A* **2001**, *105*, 880.
(14) Shaik, S. S.; Schlegel, H. B.; Wolfe, S. *Theoretical Aspects of Physical Organic Chemistry: The S_N2 reaction*; Wiley; New York, 1992.
(15) Tachibana, A. *J. Chem. Phys.* **2001**, *115*, 3497.
(16) (a) Toro-Labbé, A.; Gutiérrez-Oliva, S.; Murray, J. S.; Politzer, P. *J. Mol. Model.* **2009**, *15*, 707. (b) Toro-Labbé, A.; Gutiérrez-Oliva, S.; Murray, J. S.; Politzer, P. *Mol. Phys.* **2007**, *105*, 2619. (c) Murray, J. S.; Toro-Labbé, A.; Clark, T.; Politzer, P. *J. Mol. Model.* **2009**, *15*, 701. (d) Jaque, P.; Toro-Labbé, A.; Geerlings, P.; De Proft, F. *J. Phys. Chem. A* **2009**, *113*, 332.
(17) (a) Sears, S. B.; Parr, R. G.; Dinur, U. *Isr. J. Chem* **1980**, *19*, 165. (b) Sears, S. B.; Gadre, S. R. *J. Chem. Phys.* **1981**, *75*, 4626. (c) Koga, T.; Morita, M. *J. Chem. Phys.* **1983**, *79*, 1933. (d) Ghosh, S. K.; M.; Berkowitz; Parr, R. G. *Proc. Natl. Acad. Sci. U.S.A.* **1984**, *81*, 8028. (e) Gadre, S. R.; Sears, S. B.; Chakravorty, S. J.; Bendale, R. D. *Phys. Rev. A* **1985**, *32*, 2602. (f) Angulo, J. C.; Dehesa, J. S. *J. Chem. Phys.* **1992**, *97*, 6485. (g) Antolín, J.; Zarzo, A.; Angulo, J. C. *Phys. Rev. A* **1993**, *48*, 4149. (h) Angulo, J. C. *Phys. Rev. A* **1994**, *50*, 311. (i) Tripathi, A. N.; Smith, V. H., Jr.; Sagar, R. P.; Esquivel, R. O. *Phys. Rev. A* **1996**, *54*, 1877. (j) Massen, S. E.; Panos, C. P. *Phys. Lett. A* **1998**, *246*, 530. (k) Ramirez, J. C.; Perez, J. M. H.; Sagar, R. P.; Esquivel, R. O.; Ho, M.; Smith, V. H., Jr. *Phys. Rev. A* **1998**, *58*, 3507. (l) Nalewajski, R. F.; Parr, R. G. *J. Phys. Chem. A* **2001**, *105*, 7391. (m) Nalewajski, R. *Chem. Phys. Lett.* **2003**, *375*, 196. (n) Nalewajski, R. F. *Int. J. Mol. Sci.* **2002**, *3*, 237. (o) Nagy, A. *J. Chem. Phys.* **2003**, *119*, 9401. (p) Romera, E.; Dehesa, J. S. *J. Chem. Phys.* **2004**, *120*, 89069. (q) Karafiloglou, P.; Panos, C. P. *Chem. Phys. Lett.* **2004**, *389*, 400. (r) Sen, K. D. *J. Chem. Phys.* **2005**, *123* (1−9), 074110. (s) De Proft, F.; Ayers, P. W.; Sen, K. D.; Geerlings, P. *J. Chem. Phys.* **2004**, *120*, 9969. (t) Sen, K. D.; De Proft, F.; Borgoo, A.; Geerlings, P. *Cem. Phys. Lett.* **2005**, *410*, 70. (u) Parr, R. G.; Nalewajski, R. F.; Ayers, P. W. *J. Phys. Chem. A* **2005**, *109*, 3957. (v) Guevara, N. L.; Sagar, R. P.; Esquivel, R. O. *J. Chem. Phys.* **2005**, *122*, 084101. (w) Shi, Q.; Kais, S. *J. Chem. Phys.* **2005**, *309*, 127. (x) Chatzisavvas, K. Ch.; Moustakidis, Ch. C.; Panos, C. P. *J. Chem. Phys.* **2005**, *123*, 174111. (y) Sen, K. D.; Katriel, J. *J. Chem. Phys.* **2006**, *125* (1−4), 074117. (z) Nagy, A. *Chem. Phys. Lett.* **2006**, *425*, 154. (aa) Ayers, W. *Theor. Chem. Acc.* **2006**, *115*, 253. (bb) Martyusheva, L. M.; Seleznev, V. D. *Phys. Rep.* **2006**, *426*, 1. (cc) Liu, S. *J. Chem. Phys.* **2007**, *126* (1−3), 191107. (dd) Janssens, S.; Borgoo, A.; Van Alsenoy, C.; Geerlings, P. *J. Phys. Chem. A* **2008**, *112*, 10560. (ee) Sagar, R. P.; Laguna, H. G.; Guevara, N. L. *Mol. Phys.* 2009.
(18) (a) Esquivel, R. O.; Flores-Gallegos, N.; Carrera, E. Iuga, C.;; Angulo, J. C.; Antolín, J. *Theor. Chem. Acc.* **2009**, *124*, 445. (b) Esquivel, R. O.; Flores-Gallegos, N.; Iuga, C.; Carrera, E.; Angulo, J. C.; Antolín, J. *Phys. Lett. A* **2009**, DOI: 10.1016/j. physleta. 2009.12.018.
(19) Jasinski, J. M.; Estes, R. D. *Chem. Phys. Lett.* **1985**, *117*, 495.
(20) Perkins, G. G. A.; Lampe, F. W. *J. Am. Chem. Soc.* **1980**, *102*, 3764.
(21) (a) Jasinski, J. M.; Becerra, R.; Walsh, R. *Chem. Rev.* **1995**, *95*, 1203. (b) Becerra, R.; Walsh., R. In *Research in chemical kinetics*; Compton, R. G., Hancock, G., Eds.; Elsevier: Amsterdam, 1995; Vol. 3, p 263.
(22) (a) Gordon, M. S. *J. Chem. Soc. Chem. Commun.* **1981**, 890. (b) Grev, R. S.; Schaefer, H. F., III. *J. Chem. Soc. Chem. Commun.* **1983**, 785. (c) Sosa, C.; Schlegel, H. B. *J. Am. Chem. Soc.* **1984**, *106*, 5847. (d) Sax, A.; Olbrich, G. *J. Am. Chem. Soc.* **1985**, *107*, 4868. (e) Gordon, M. S.; Gano, D. R.; Binkley, J. S.; Frisch, M. J. *J. Am. Chem. Soc.* **1986**, *108*, 2191.
(23) (a) Becerra, R.; Boganov, S. E.; Egorov, M. P.; Faustov, V. I.; Nefedov, O. M.; Walsh, R. *Can. J. Chem.* **2000**, *78*, 1428. (b) Becerra, R.; Frey, H. M.; Mason, B. P.; Walsh, R. *J. Organomet. Chem.* **1996**, *521*, 343.
(24) Shannon, C. E. *Bell Syst. Tech. J.* **1948**, *27*, 379.
(25) Bialynicky-Birula, I.; Mycielski, J. *Commun. Math. Phys.* **1975**, *44*, 129.
(26) Politzer, P.; Truhlar, D. G. *Chemical Applications of Atomic and Molecular Electrostatic Potentials*; Academic Press: New York, 1981.
(27) Breneman, M.; Wiberg, K. B. *J. Comput. Chem.* **1990**, *11*, 361.
(28) Stone, A. J.; Alderton, M. *Mol. Phys.* **1985**, *56* (5)), 1047.
(29) (a) Parr, R. G.; Pearson, R. G. *J. Am. Chem. Soc.* **1983**, *105*, 7512. (b) Parr, R. G.; Yang, W. *Density-Functional Theory of Atoms and Molecules*; Oxford University Press; New York, 1989; (c) Geerlings, P.;

De Proft, F.; Langenaeker, W. *Chem. Rev.* **2003**, *103* (5), 1793. (d) THEOCHEM special issue *Conceptual Insight from Density Functional Theory*; Chattaraj, P. K., Thakkar, A. J., Eds.; 2009.

(30) (a) Koopmans, T. A. *Physica* **1933**, *1*, 104. (b) Janak, J. F. *Phys. Rev B* **1978**, *18*, 7165.

(31) (a) Ayers, P. W.; Parr, R. G.; Pearson, R. G. *J. Chem. Phys.* **2006**, *124*, 194107. (b) Pearson, R. G. *Inorg. Chim. Acta* **1995**, *240*, 93.

(32) (a) Ghanty, T. K.; Ghosh, S. K. *J. Phys. Chem.* **1993**, *97*, 4951. (b) Roy, R.; Chandra, A. K.; Pal, S. *J. Phys. Chem.* **1994**, *98*, 10447. (c) Hati, S.; Datta, D. *J. Phys. Chem.* **1994**, *98*, 10451. (d) Simon-Manso, Y.; Fuenteaelba, P. *J. Phys. Chem. A* **1998**, *102*, 2029.

(33) Chattaraj, P. K.; Sarkar, U.; Roy, D. R. *Chem. Rev.* **2006**, *106*, 2065.

(34) (a) Pearson, R. G. *J. Am. Chem. Soc.* **1963**, *85*, 3533. (b) Pearson, R. G. *Hard and Soft Acids and Bases*; Dowen, Hutchinson and Ross: Stroudsberg, 1973; (c) Pearson, R. G. *Chemical Hardness*; Wiley-VCH: New York, 1997.

(35) Ayers, P. W. *Faraday Discuss.* **2007**, *135*, 161.

(36) *Gaussian 03, Revision D.01*, Frisch, M. J.; Trucks, G. W.; Schlegel, H. B.; Scuseria, G. E.; Robb, M. A.; Cheeseman, J. R.; Montgomery Jr., J. A.; Vreven, T.; Kudin, K. N.; Burant, J. C.; Millam, J. M.; Iyengar, S. S.; Tomasi, J.; Barone, V.; Mennucci, B.; Cossi, M.; Scalmani, G.; Rega, N.; Petersson, G. A.; Nakatsuji, H.; Hada, M.; Ehara, M.; Toyota, K.; Fukuda, R.; Hasegawa, J.; Ishida, M.; Nakajima, T.; Honda, Y.; Kitao, O.; Nakai, H.; Klene, M.; Li, X.; Knox, J. E.; Hratchian, H. P.; Cross, J. B.; Bakken, V.; Adamo, C.; Jaramillo, J.; Gomperts, R.; Stratmann, R. E.; Yazyev, O.; Austin, A. J.; Cammi, R.; Pomelli, C.; Ochterski, J. W.; Ayala, P. Y.; Morokuma, K.; Voth, G. A.; Salvador, P.; Dannenberg, J. J.; Zakrzewski, V. G.; Dapprich, S.; Daniels, A. D.; Strain, M. C.; Farkas, O.; Malick, D. K.; Rabuck, A. D.; Raghavachari, K.; Foresman, J. B.; Ortiz, J. V.; Cui, Q.; Baboul, A. G.; Clifford, S.; Cioslowski, J.; Stefanov, B. B.; Liu, G.; Liashenko, A.; Piskorz, P.; Komaromi, I.; Martin, R. L.; Fox, D. J.; Keith, T.; Al-Laham, M. A.; Peng, C. Y.; Nanayakkara, A.; Challacombe, M.; Gill, P. M. W.; Johnson, B.; Chen, W.; Wong, M. W.; González, C.; Pople, J. A. 2004, Gaussian, Inc., Wallingford CT.

(37) (a) Pérez-Jordá, J. M.; San-Fabián, E. *Comput. Phys. Commun.* **1993**, *77*, 46. (b) Pérez-Jordá, J. M.; Becke, A. D.; San-Fabián, E. *J. Chem. Phys.* **1994**, *100*, 6520.

(38) Kohout, M. *Program DGRID version 4.2*, 2007.

(39) Schaftenaar, G.; Noordik, J. H. *MOLDEN*: A pre- and post-processing program for molecular and electronic structure. *J. Comput.-Aided Mol. Design* **2000**, *14*, 123.

(40) (a) Kollmar, H. *J. Am. Chem. SOC.* **1978**, *100*, 2660. (b) Jeziorek, D.; Zurawski, B. *Int. J. Quantum Chem.* **1979**, *16*, 277.

(41) (a) Grev, R. S.; Schaefer, H. F., III. *J. Chem. Soc. Chem. Commun.* **1983**, 785. (b) Sosa, C.; Lee, C. *J. Chem. Phys.* **1983**, *98*, 8004.

(42) Jasinski, M. J. M. *J. Phys. Chem.* **1986**, *90*, 555.

(43) (a) Gordon, M. S.; Gano, D. R. *J. Am. Chem. Soc.* **1984**, *106* (19), 5421. (b) Sosa, C.; Lee, C. *J. Chem. Phys.* **1993**, *98*, 8004. (c) Bowrey, M.; Purnell, J. H. *J. Am. Chem. Soc.* **1970**, *92* (8), 2594.

(44) Polanyi, J. C.; Zewail, A. H. *Acc. Chem. Res.* **1995**, *28*, 119.

(45) Pennini, P.; Plastino, A. *Phys. Lett. A* **2007**, *365*, 263.

(46) Shaik, S. S. *New J. Chem.* **2007**, *31*, 2015.

JP908898W